Journal of Crystal Growth 600 (2022) 126915

Contents lists available at ScienceDirect

Journal of Crystal Growth

journal homepage: www.elsevier.com/locate/jcrysgro

Physical-Vapor-Transport growth of 4H silicon carbide single crystals by a tiling method

Naifu Zhang [a,b], Yue Gao [a,b], Ruzhong Zhu [a,b], Rong Wang [a,b,*], Deren Yang [a,b], Xiaodong Pi [a,b,*]

[a] State Key Laboratory of Silicon Materials & School of Materials Science and Engineering, Zhejiang University, Hangzhou 310027, China

[b] Institute of Advanced Semiconductors & Zhejiang Provincial Key Laboratory of Power Semiconductor Materials and Devices, ZJU-Hangzhou Global Scientific and Technological Innovation Center, Zhejiang University, Hangzhou 310027, China

ARTICLE INFO

Communicated by Matthias Bickermann

Keywords:
A1. Point defects
A2. Growth from vapor
A2. Seed crystals
A2. Single crystal growth
B2. Semiconducting silicon compounds

ABSTRACT

Increasing the diameter and reducing the dislocation density of 4H silicon carbide (4H-SiC) single crystals are the development tendency of 4H-SiC single-crystal substrate to reduce the cost of 4H-SiC based devices. In this work, we use the growth of a 100 mm 4H-SiC single crystal as an example to demonstrate that the tiling approach is attractive to enlarge the diameter of physical-vapor-transport (PVT)-grown 4H-SiC single crystals by a single growth period. By titling four pieces of 4H-SiC seed crystals, a 100 mm 4H-SiC boule without crystal deterioration is obtained by the PVT growth method. The shape of the growth interface is convex and complete after the PVT growth, indicating the tiling gaps between neighboring seed-crystal pieces are healed after the PVT growth of 25-mm thick 4H-SiC. Wafers are obtained after sequential slicing, lapping, and chemical mechanical polishing (CMP). The high-resolution X-ray diffraction (HRXRD) rocking curve measurements of the wafer at the latest growth stage indicate that the 4H-SiC crystal is basically healed, with mesoscopic boundaries being created at the central area of the wafer. Raman spectra indicate that the healing polymorph across the tiling gaps is 4H-SiC. We find that threading edge dislocations (TEDs) dominate the dislocation types in the 4H-SiC substrate wafers at the initial, middle, and latest growth stages. As the PVT growth proceeds, the density of dislocations in 4H-SiC wafers significantly decreases, as a result of the crystalline healing. Our work opens a pathway to enlarge the size of 4H-SiC single crystals in a single PVT growth period, which paves the way for the high-efficiency growth of large-size 4H-SiC single-crystals.

1. Introduction

4H-SiC holds great promise for the development of high-frequency and high-power electronic devices, owing to its superior properties of wide bandgap, high breakdown electric field strength, and high thermal conductivity [1–3]. High-quality 4H-SiC single-crystal substrates are the basis of high-performance 4H-SiC based electronic devices. Driven by reducing the cost and promoting the performance of a 4H-SiC based electronic device, researchers have devoted a long time to increase the diameter and reduce the dislocation density of 4H-SiC single crystals.

The PVT technology is the most well-developed 4H-SiC growth technique, due to the advantages of the sensitive-temperature tunability, and low cost of the solid raw materials. At present, PVT-grown 150 mm 4H-SiC single crystals have been widely industrialized, lab-scale 200 mm 4H-SiC single crystals have already been realized [4]. Traditionally, increasing the diameter of a PVT-grown 4H-SiC single crystal is slowly achieved by promoting the lateral crystal growth with specially designed thermal fields [5–7]. This approach suffers from the drawbacks of poor efficiency, high cost, and limited single-crystal quality. It takes at least ten growth periods to enlarge the diameter of a 4H-SiC boule from 150 mm to 200 mm, and it takes another several growth periods to optimize the quality of the enlarged 4H-SiC boule. A more efficient method to enlarge the diameter of 4H-SiC boules is strongly desired. It has been shown that the diameter of a gallium nitride crystal can be enlarged to 175 mm by tiling 24 mm seed-crystal pieces with the hydride vapor phase epitaxy (HVPE) method [8–10]. This opens a pathway to enlarge the diameter of single crystals by the tiling approach.

In this work, we use the growth of a 100 mm 4H-SiC single crystal as an example to demonstrate that the tiling approach is attractive to

* Corresponding authors at: State Key Laboratory of Silicon Materials & School of Materials Science and Engineering, Zhejiang University, Hangzhou 310027, China.

E-mail addresses: rong_wang@zju.edu.cn (R. Wang), xdpi@zju.edu.cn (X. Pi).

https://doi.org/10.1016/j.jcrysgro.2022.126915
Received 14 August 2022; Received in revised form 5 October 2022; Accepted 7 October 2022
Available online 14 October 2022
0022-0248/© 2022 Elsevier B.V. All rights reserved.

enlarge the diameter of PVT-grown 4H-SiC single crystals by a single growth period. By titling four pieces of 4H-SiC seed crystals, a 100 mm 4H-SiC boule without crystal deterioration is obtained by the PVT growth method. The shape of the growth interface is convex and complete after the PVT growth, indicating the tiling gaps between neighboring seed-crystal pieces are healed after the PVT growth of 25-mm thick 4H-SiC. Wafers are obtained after sequential slicing, lapping and CMP. The high-resolution X-ray diffraction (HRXRD) rocking curve measurements of the wafer at the latest growth stage indicate that the 4H-SiC crystal is completely healed, with mesoscopic boundaries being created at the central area of the wafer. Raman spectra indicate that the healing polymorph across the tiling gaps is 4H-SiC. We find that threading edge dislocations (TEDs) dominate the dislocation types in the 4H-SiC substrate wafers at the initial, middle, and latest growth stages. The density of TEDs along the $[11\overline{2}0]$ direction is higher than that along the $[\overline{1}100]$ direction, as a result of reduced cross-slip through TED-basal plane dislocation (BPD) transitions. As the PVT growth proceeds, the density of dislocations in 4H-SiC wafers significantly decreases, as a result of the crystalline healing. Our work indicates that the tiling approach is capable of enlarge the size of PVT-grown 4H-SiC single crystals, and paves the way for the growth of 4H-SiC single-crystals above 200 mm.

2. Experiment

The fundamental seeds are extracted from our home-made 75 mm 4H-SiC substrates by laser cutting. We design the fundamental seed form as a one-fourth circle. Their side lengths are 50 mm each. As shown in Fig. 1a, the laser cutting is carried out along the crystal orientation of $[\overline{1}100]$ and $[11\overline{2}0]$, which is defined as Type A and Type M, respectively. The tiling of the seed-crystal pieces is carried out by putting the same type of gaps together. Then, seed-crystal pieces are inserted into the four-inch hoop of the laminating machine, and a plastic film is applied to the seed crystal to seal the pieces together. The plastic film is ripped off after the seed-crystal is bonded to the graphite holder with a high-temperature adhesive. A 4H-SiC boule was grown on the titling seed crystal by the PVT method. The growth temperature was set between 2000 and 2300 °C. The growth pressure was maintained between 0.1 and 1.0 kPa. The growth process is schematically shown in Fig. 1b. We firstly grew a 4H-SiC boule with an approximate thickness of 10 mm on the C face of the tiled seed crystal. The 10 mm 4H-SiC boule was then used as the seed crystal for the second growth after fine grounding of its C face. 4H-SiC substrates were prepared from the 4H-SiC boule by a standard wafering process, including slicing, lapping, and CMP. Three wafers, labeled as A, B, and C, were chosen to investigate the properties of 4H-SiC wafers at the early, middle, and late growth stages, respectively. Wafer A, B, and C are obtained from the 4H-SiC boule grown in the second growth experiment. All the characterizations were carried out on the Si face of the 4H-SiC wafers.

The surface morphologies and tiling-interface morphologies were characterized by the Olympus-BX53M optical microscopy (OM) and Zeiss Sigma300 scanning electron microscopy (SEM). Raman scattering spectroscopy was conducted at room temperature using the Witec RAS300 Raman Spectrometer with a laser at 532 nm used for excitation. The HRXRD rocking curve measurements were performed on the XPert III MRD XRD diffractometer operating with Cu $K_{\alpha 1}$ radiation. Molten KOH etching at 550 ℃ was employed to reveal dislocations [11]. The identification of dislocations was carried out by discriminating the shape and size of the molten-KOH etch pits. And the automated etch feature counting was accomplished by a FabXLab optical microscope with automatic image recognition.

3. Results and discussion

Fig. 2a shows the optical picture of the first grown 10 mm-thick 4H-SiC boule. It is clear that the tiling gaps of neighboring seed parts transforms into mesoscopic boundaries, micropipes (MPs), and completely heal during the PVT growth. As shown in Fig. 2b, the healing across the tiling gaps is inhomogeneous. The healing of tiling gaps is driven by the gradual filling of 4H-SiC species into the tiling gaps during the PVT growth. Since the tiling gaps tend to be healed during the first growth, we then use the 10 mm 4H-SiC boule as the seed crystal for the second growth.

Fig. 3a displays the optical picture of the 25 mm-thick 4H-SiC boule after the second growth. The complete and convex 4H-SiC boule is achieved after the second growth. Macroscopically, the second growth of 15 mm-thick 4H-SiC completely heals the tiling gaps between neighboring seed crystals. 4H-SiC wafers are obtained by sequential slicing, lapping, and CMP. Three wafers, labeled as A, B, and C, were chosen to investigate the properties of 4H-SiC wafers at the early, middle, and late growth stages, respectively. For Wafer C at the latest growth stage, we find that stitching traces cannot be observed at most parts of the 4H-SiC wafer (Fig. 3b). Only four connecting interfaces are observed under OM at the central region of the Wafer C. At the central region, the healing of tiling gaps is achieved by filling the gaps both along both $[\overline{1}100]$ and $[11\overline{2}0]$ directions. The decussation of these two tiling gaps poses an additional challenge for the healing process. As shown in Fig. 3c and d, the tiling boundaries along $[11\overline{2}0]$ and $[\overline{1}100]$ at the central region of wafer C present as linear boundary and butterfly boundaries, which indicates different healing behaviors along these directions. Scanning electron microscopy is applied to evaluate the cross-section of the wafers with regard to the early and later growth stages. A

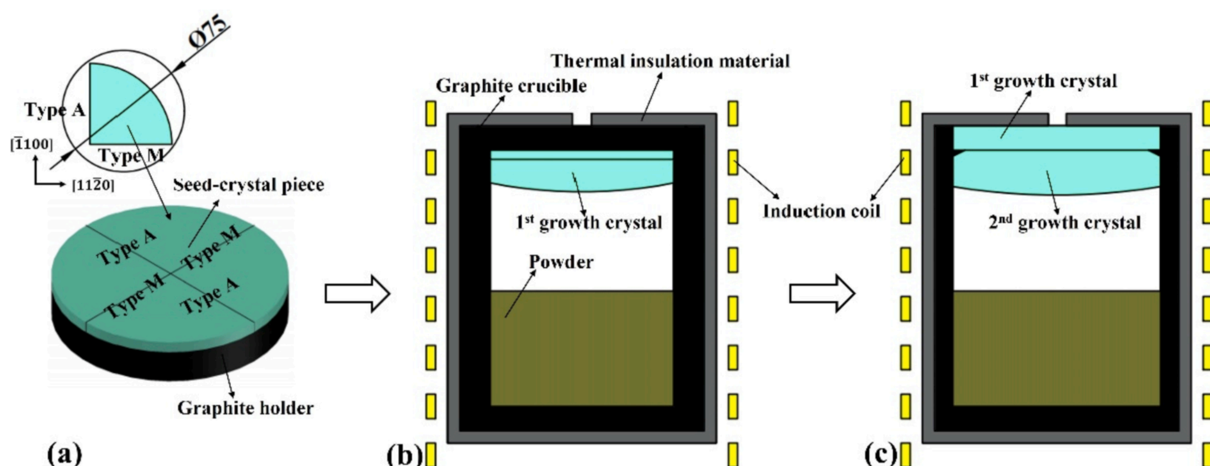

Fig. 1. The schematic diagram showing the (a) seed-tiling approach, (b) first 4H-SiC single-crystal growth, and (c) the second 4H-SiC single-crystal growth.

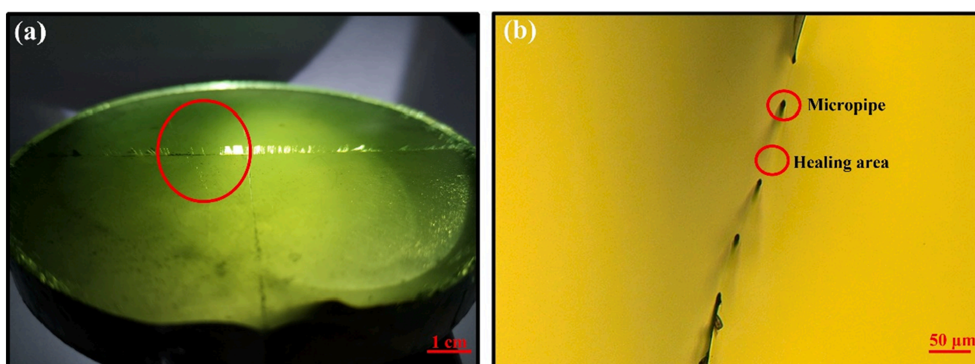

Fig. 2. Optical image of (a) the first as-grown 4H-SiC boule, (b) OM image of the red-circle marked area of (a) in the transmission mode. (For interpretation of the references to color in this figure legend, the reader is referred to the web version of this article.)

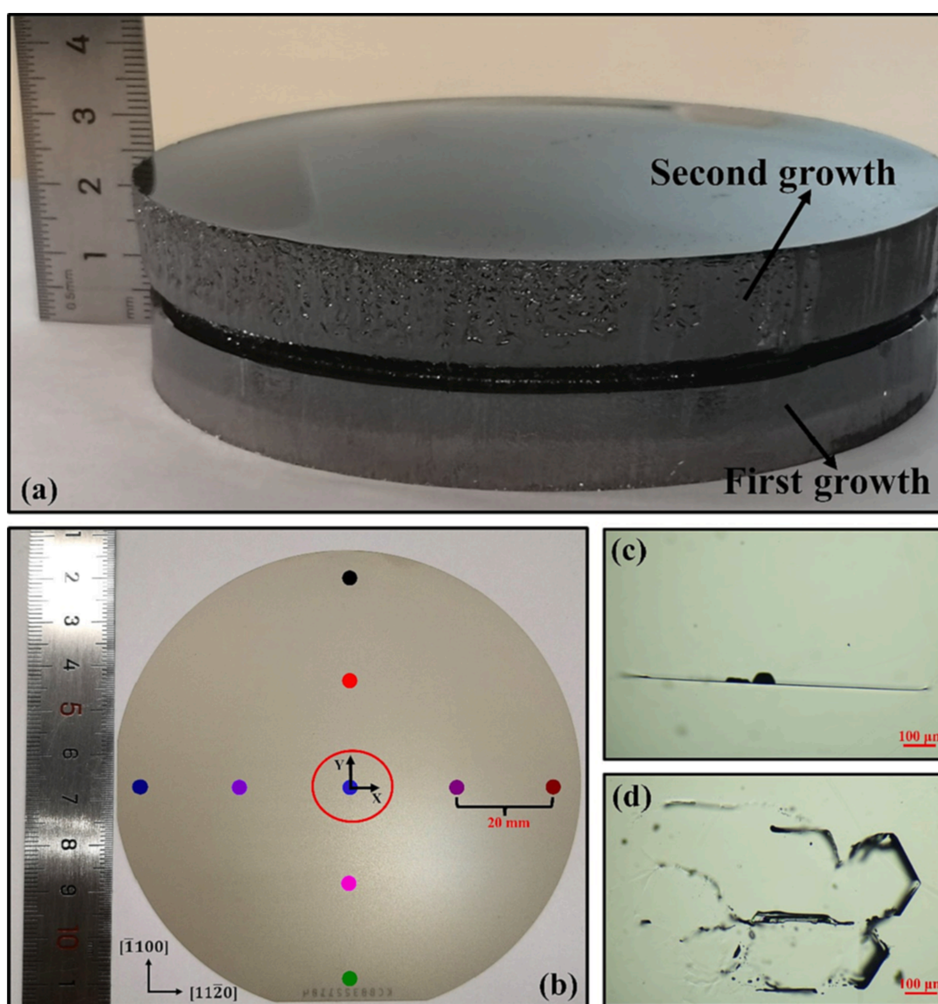

Fig. 3. Optical image of (a) the as-grown 4H-SiC boule after the second growth, (b) Wafer C, (c) linear boundaries along [11$\bar{2}$0] at the red-circle region of Wafer C, and (d) butterfly boundaries along [$\bar{1}$100] at the red-circle region of Wafer C. (For interpretation of the references to color in this figure legend, the reader is referred to the web version of this article.)

clear healing process (Fig. S2 in the supplementary material) can be observed when compared to the wafer edge of the seed-crystal piece following laser cutting (Fig. S1 in the supplementary material). However, nearly all of the initial growth stage's unhealed gaps are inherited to the later stage (Fig. S3 in the supplementary material), presumably as a result of insufficient healing time. What's more, wafers of different growth stages indicate that the healing difficulty of the gaps in the central area is not anisotropic.

XRD rocking-curve measurements are then carried out to evaluate the crystalline characters of Wafers A, B, and C. As shown in Fig. 3b, XRD rocking-curve measurements were taken at 9 points along the tiling seams of each wafer. At the initial growth stage (Wafer A), the XRD rocking curves at positions of (0, 0), (0, −20), (−40, 0) and (40, 0) exhibit a clear peak splitting (Fig. 4a), which indicates that there are

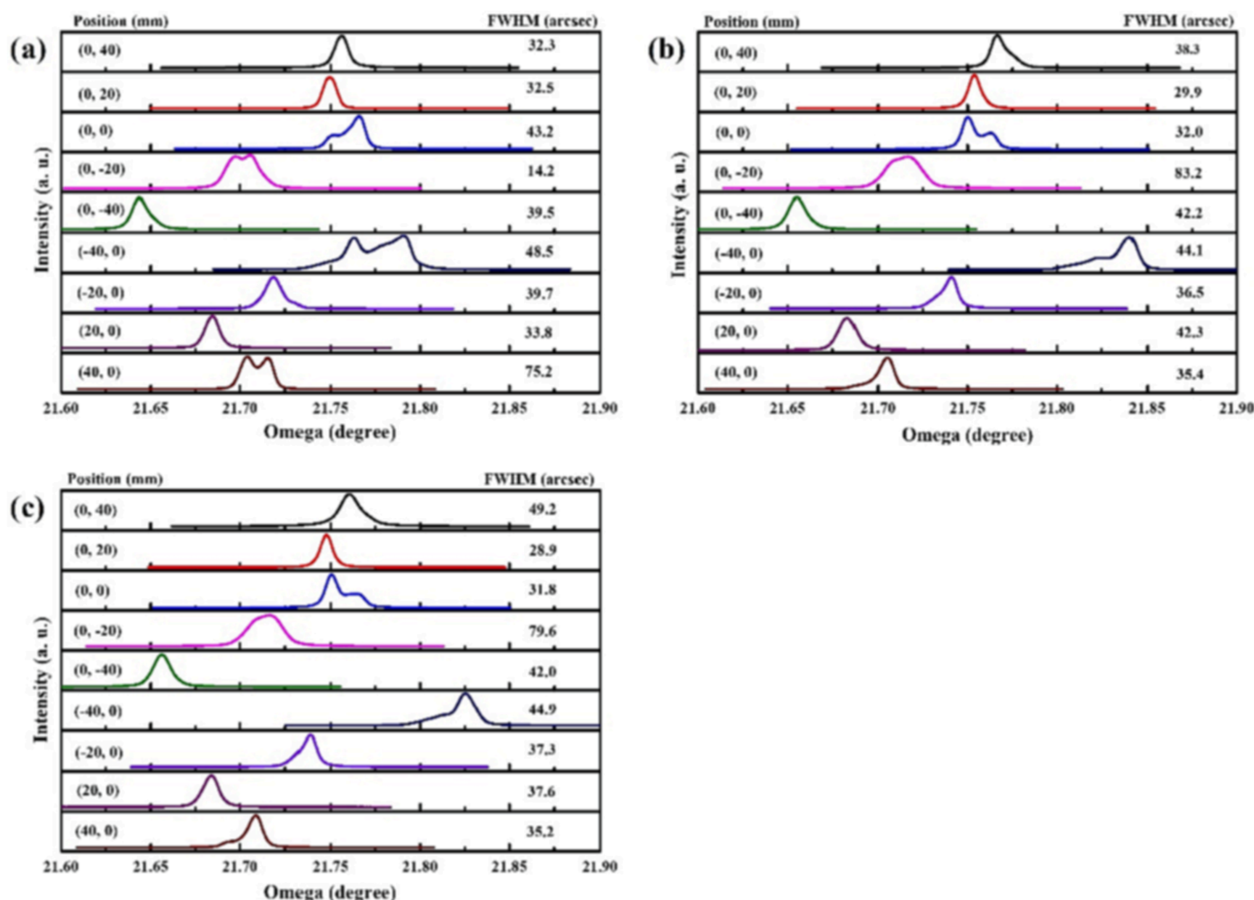

Fig. 4. The off-axis SiC (0004) ω-XRCs of (a) Wafer A, (b) Wafer B, and (c) Wafer C.

domain boundaries or twin boundaries at these regions. The number of peak splitting along $[11\bar{2}0]$ direction is larger than that along $[\bar{1}100]$ direction. It is known that the growth rate of 4H-SiC along the $[\bar{1}100]$ direction is slower than that along the $[11\bar{2}0]$ direction [12]. Therefore, the anisotropic numbers of peak splitting may be relevant to the slow-healing induced tiling gaps. However, further research is needed to determine whether the degree of interface repair difficulty is influenced by crystal orientation or by sporadic elements during the tiling process. All XRCs display a single peak in the later stages of growth except for the central region (Fig. 4c), suggesting that the boundaries or twins would progressively vanish as growth proceeded.

Numerous tests have demonstrated that the primary influences on SiC polytypes are seed polarity, growth temperature, and gas phase Si/C atomic ratio. We can ensure that the 4H-SiC will be grown in accordance with the accepted growth conditions, and other factors influencing the polytypes can be excluded in addition to tiling. The Raman spectra is then used to evaluate the polymorph of the grown 4H-SiC. The 9-point Raman spectra of Wafer A are shown in Fig. 5. Three Raman active vibrational modes locating at 204 cm^{-1}, 776 cm^{-1}, 964 cm^{-1} are observed, which correspond to the folded modes of transverse acoustic (FTA), transverse optic (FTO), and longitudinal optic (FLO) branches, respectively. The peak positions of the all branches agree well with that of 4H-SiC [13–15]. The polytype of the measured crystal can be identified by the clear variation in Raman spectrum strength [13]. The hexagonal percentage of 4H-SiC is 50 %, i.e., the FTA and FTO with the reduced wave vector of 1/2 should have the highest strength, which is precisely the same as the result shown in Fig. 5. These two factors indicate that the polymorph of 4H is well kept during the filling of tiling gaps and growth of the 4H-SiC boule. We note that the Raman spectra of all points of Wafer A, B, and C are identical to each other, indicating that

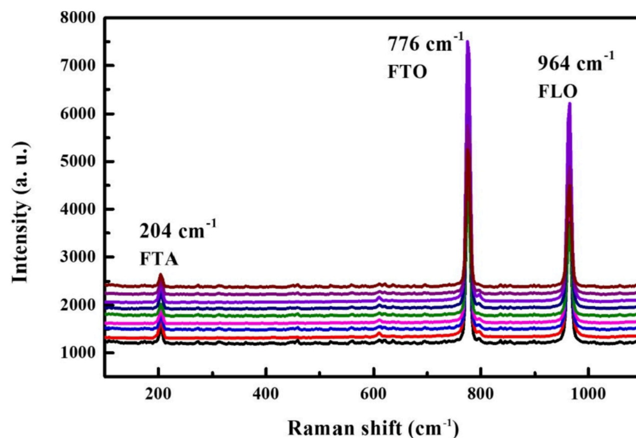

Fig. 5. The Raman spectra of Wafer A. Taking 9 points for 20 mm steps along the tiling boundary. The color of each line is consistent with the color of the point in Fig. 3b.

polymorph transition does not occur during the PVT-growth of 4H-SiC boule by the tiling method.

At last, we use the molten-KOH etching to reveal the dislocation density of Wafers A, B, and C. According to previous discriminating approaches, the sea-shell shaped, larger hexagonal, and smaller hexagonal etch pits correspond to the etch pits of BPDs, TSDs, and TEDs, respectively [16]. Fig. 6a displays the surface morphology of a molten-KOH etched 4H-SiC sample. It should be noted that although TSD has a round morphology and the corrosion conditions still need to be

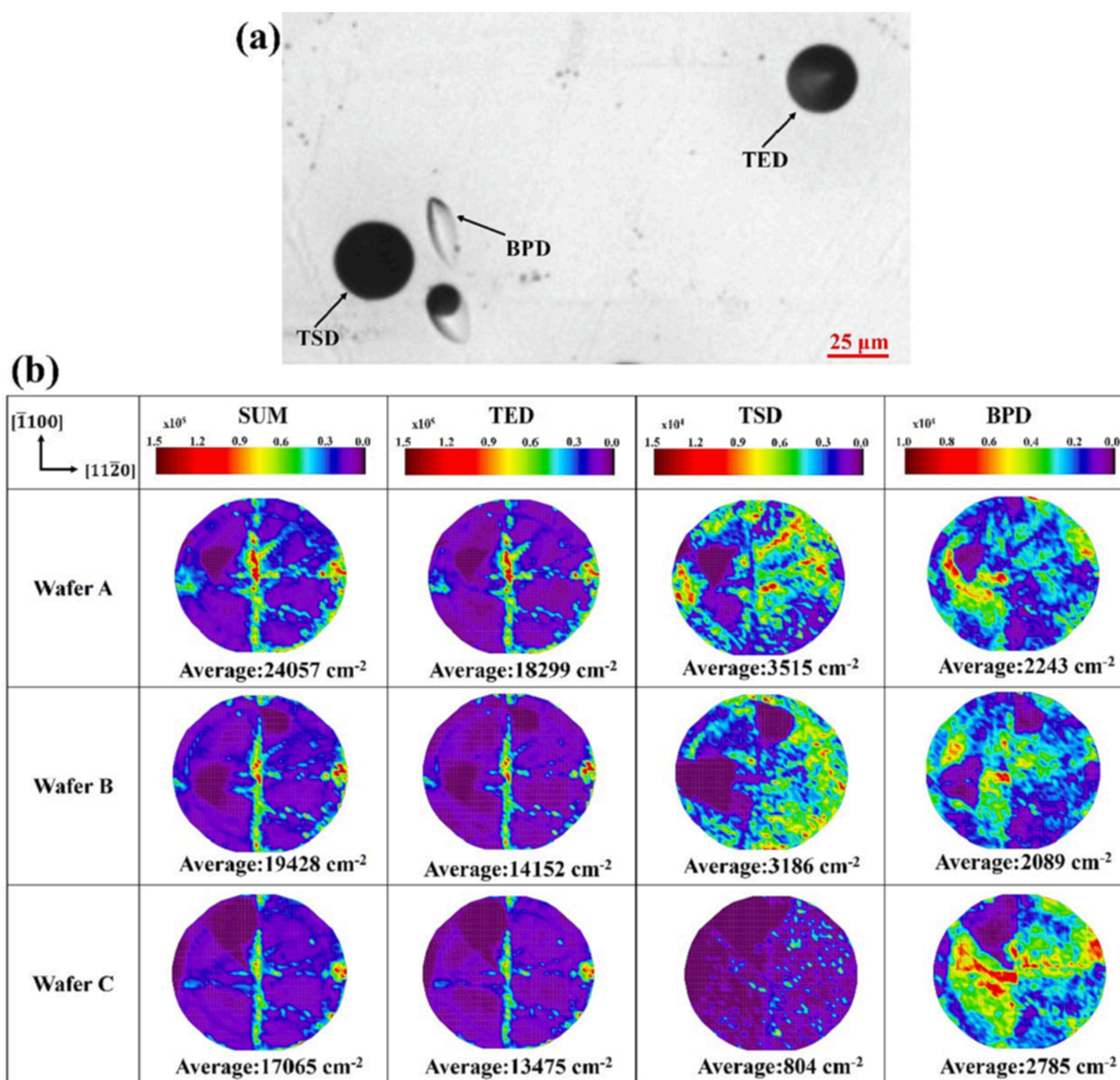

Fig. 6. (a) Representative OM image showing the morphology of the etch pits of different dislocations, (b) Wafer-scale distribution of dislocation densities of Wafer A, Wafer B, and Wafer C.

improved, this does not affect its recognition. Dislocation distributions of the whole wafer in all samples are counted with automatic image recognition according to the etch pit morphology of different dislocations (Fig. 6b). The distributions of dislocations of Wafers A, B, and C are similar to each other, and the density of TEDs is the highest among all the dislocation types. It is clear that TEDs tend to accumulate at the tiling gap along the [$1\overline{1}00$] direction, while the accumulation of TEDs along [$11\overline{2}0$] direction is not obvious. We note that the generation of BPDs is caused by relieving the stress during the filling of the tiling gap between neighboring seed crystals along the directions of both [$11\overline{2}0$] and [$1\overline{1}00$]. However, it is well known that TEDs are capable of transforming to BPDs on the {$\overline{1}100$} prismatic plane during the PVT growth [3]. We speculate that the opposite conversion process took place in this experiment, resulting in an increase of TEDs along the [$\overline{1}100$]. In contrast, the BPDs density along the [$11\overline{2}0$] direction is higher than that along the [$\overline{1}100$] direction. Once upon the transition, BPDs along the [$11\overline{2}0$] direction can easily slip along the growth steps towards the outside of the 4H-SiC boule. The increased BPD density at the downstream of the growth direction verified the explanation (BPD density of Wafer C in Fig. 6b). We note that the densities of BPDs of Wafer A and Wafer B are lower than that of Wafer C, because at the early and middle growth stages, BPDs are capable of growing outside the 4H-SiC single crystal via the growth steps [17]. The distribution of TSDs across the wafer is more homogeneous than that of TEDs and BPDs. As the PVT growth proceeds, the densities of TEDs and TSDs both decrease, as a result of the healing of tiling gaps.

4. Conclusion

In conclusion, a 100 mm 4H-SiC single crystal is grown by tiling 4 pieces of seed-crystal pieces. The HRXRD rocking curve measurements of the wafer at the latest growth stage indicate that the 4H-SiC crystal is basically healed, with mesoscopic boundaries being created at the central area of the wafer. Raman spectra indicate that the healing polymorph across the tiling gaps is 4H-SiC. We find that TEDs dominate the dislocation types in the 4H-SiC substrate wafers at the initial, middle, and latest growth stages. The density of TEDs along the [$11\overline{2}0$] direction is higher than that along [$\overline{1}100$] direction, as a result of reduced cross-slip through TED- BPD transitions. As the PVT growth proceeds, the density of dislocations in 4H-SiC wafers significantly decreases, as a result of the crystalline healing. Our work indicates that the tiling approach is capable of enlarging the size of PVT-grown 4H-SiC single crystals, and paves the way for the growth of 4H-SiC single-crystals above 200 mm.

CRediT authorship contribution statement

Naifu Zhang: Conceptualization, Investigation, Writing – original draft. **Yue Gao:** Investigation. **Ruzhong Zhu:** Investigation. **Rong Wang:** Writing – original draft. **Deren Yang:** Funding acquisition. **Xiaodong Pi:** Funding acquisition, Writing – original draft, Supervision.

Declaration of Competing Interest

The authors declare that they have no known competing financial interests or personal relationships that could have appeared to influence the work reported in this paper.

Data availability

Data will be made available on request.

Acknowledgement

This work is supported by “Pioneer” and “Leading Goose” R&D Program of Zhejiang (Grant No. 2022C01021) and Natural Science Foundation of China (Grant Nos. 91964107 and U20A20209).

Appendix A. Supplementary material

Supplementary data to this article can be found online at https://doi.org/10.1016/j.jcrysgro.2022.126915.

References

[1] P.J. Wellmann, Review of SiC crystal growth technology, Semicond. Sci. Technol. 33 (10) (2018) 103001.
[2] R. Tian, et al., A review of manufacturing technologies for silicon carbide superjunction devices, J. Semicond. 42 (2021), 061801.
[3] D. Chaussende, N. Ohtani, 5-Silicon carbide, Woodhead Publishing, Single Crystals of Electronic Materials, 2019, pp. 129–179.
[4] A.R. Powell, J.J. Sumakeris, Y. Khlebnikov, M.J. Paisley, R.T. Leonard, E. Deyneka, S. Gangwal, J. Ambati, V. Tsevtkov, J. Seaman, A. McClure, C. Horton, O. Kramarenko, V. Sakhalkar, M. O'Loughlin, A.A. Burk, J.Q. Guo, M. Dudley, E. Balkas, Bulk growth of large area SiC crystals, Mater. Sci. Forum 858 (2016) 5–10.
[5] S. Lin, Z. Chen, D. Jiang, P. Liang, J. Wan, B.o. Liu, H. Xie, X. Feng, A technique for diameter enlargement in SiC crystal growth, Int. J. Mater. Res. 101 (12) (2010) 1514–1518.
[6] T. Kato, T. Miura, I. Nagai, H. Taniguchi, H. Kawashima, T. Ozawa, K. Arai, H. Okumura, Enlargement growth of large 4H-SiC bulk single crystal, Mater. Sci. Forum 679-680 (2011) 3–7.
[7] Y. Shi, X. Yang, D. Wang, P. Zhang, J. Zhang, Y. Hao, J. Yang, Enlargement of silicon carbide lely platelet by physical vapor transport technique, Mater. Manuf. Processes 28 (11) (2013) 1248–1252.
[8] T. Yoshida, et al., Development of GaN substrate with a large diameter and small orientation deviation, Phys. Status Solidi B 8 (2017) 1600671.
[9] M. Imanishi, et al., Promotion of lateral growth of GaN crystals on point seeds by extraction of substrates from melt in the Na-flux method, Appl. Phys Express 12 (2019), 045508.
[10] M. Imanishi, et al., Anomalous dislocation annihilation behavior observed in a GaN crystal grown on point seeds by the Na-flux method, Appl. Phys Express 13 (2020), 085510.
[11] W.H. Geng, et al., Identification of subsurface damage of 4H-SiC wafers by combining photochemical etching and molten-alkali etching, J. Semicond. 43 (2022), 102801.
[12] N. Nordell, et al., Homoepitaxy of 6H and 4H SiC on nonplanar substrates, Appl. Phys. Lett. 72 (1998) 197.
[13] S. Nakashima, H. Harima, Raman investigation of SiC polytypes, Phys. Status Solidi A 162 (1) (1997) 39–64.
[14] C.C. Tin, R. Hu, J. Liu, Y. Vohra, Z.C. Feng, Raman microprobe assessment of low-pressure chemical vapor deposition-grown 4H-SiC epilayers, J. Cryst. Growth 158 (4) (1996) 509–513.
[15] D.C. Wang, et al., Raman analysis of epitaxial graphene on 6H-SiC (000–1) substrates under low pressure environment, J. Semicond. 32 (2011), 113003.
[16] J.J. Li, et al., Nitrogen decoration of basal-plane dislocations in 4H-SiC, Phys. Rev. Appl 17 (2022), 054011.
[17] K. Tsunenobu, et al., Defect control in growth and processing of 4h-SiC for power device applications, Mater. Sci. Forum 645–648 (2010) 645–650.